Elsevier Editorial System(tm) for Earth and Planetary Science Letters

Manuscript Draft

Manuscript Number: EPSL-D-20-00542R1

Title: Field-based Measurements of Volcanic Ash Resuspension by Wind

Article Type: Letters

Keywords: wind resuspension, wind tunnel, detachment threshold, volcanic ash, Sakurajima volcano, Cordon Caulle volcano

Corresponding Author: Dr. Elisabetta Del Bello, Ph.D.

Corresponding Author's Institution: Istituto Nazionale di Geofisica e Vulcanologia

First Author: Elisabetta Del Bello, Ph.D.

Order of Authors: Elisabetta Del Bello, Ph.D.; Jacopo Taddeucci; Jonathan P Merrison; Keld R Rasmussen; Daniele Andronico; Tullio Ricci; Piergiorgio Scarlato; Jens J Iversen

Abstract: The resuspension of volcanic ash by wind is a significant source of hazard during and after volcanic eruptions. Parameterizing and modeling ash resuspension requires direct measurement of the minimum wind shear stress required to move particles, usually expressed as the threshold friction velocity U*th, a parameter that, for volcanic ash, has been measured only scarcely and always in the laboratory. Here, we report the first field measurements of U*th for volcanic ash, with a portable wind tunnel specifically developed, calibrated, and tested. Field measurements, performed on natural reworked ash deposits from Sakurajima (Japan) and Cordón Caulle (Chile) volcanoes, agree well with our laboratory determinations on ash from the same deposits, with values of U*th ranging from 0.13 to 0.38 m/s. Our results show that the median grain size of the deposit and particle shape have a stronger control on U*th than the local substratum nature and deposit texture.

Research Data Related to this Submission

Title: Data for: Field-based Measurements of Volcanic Ash Resuspension by Wind
Repository: Mendeley Data
https://data.mendeley.com/datasets/38h7ncvyxh/draft?a=1799d4ed-6b98-46ad-a1ec-63b5182aa291

Field-based Measurements of Volcanic Ash Resuspension by Wind

E. Del Bello[1], J. Taddeucci[1], J. P. Merrison[2], K. R. Rasmussen[3], D. Andronico[4], T. Ricci[1], P. Scarlato[1], and J.J. Iversen[2]

[1]Istituto Nazionale di Geofisica e Vulcanologia, Sezione di Roma 1, Via di Vigna Murata 605, 00143, Roma, Italy.

[2]Aarhus University, Department of Physics and Astronomy, Ny Munkegade 120, 8000, Aarhus C, Denmark.

[3]Aarhus University, Department of Geoscience, Høegh-Guldbergs Gade 2, 8000, Aarhus C, Denmark.

[4]Istituto Nazionale di Geofisica e Vulcanologia, Sezione di Catania, Osservatorio Etneo, Piazza Roma 2, 95125, Catania, Italy.

Corresponding author: Elisabetta Del Bello (elisabetta.delbello@ingv.it)

Abstract

The resuspension of volcanic ash by wind is a significant source of hazard during and after volcanic eruptions. Parameterizing and modeling ash resuspension requires direct measurement of the minimum wind shear stress required to move particles, usually expressed as the threshold friction velocity U^*_{th}, a parameter that, for volcanic ash, has been measured only scarcely and always in the laboratory. Here, we report the first field measurements of U^*_{th} for volcanic ash, with a portable wind tunnel specifically developed, calibrated, and tested. Field measurements, performed on natural reworked ash deposits from Sakurajima (Japan) and Cordón Caulle (Chile) volcanoes, agree well with our laboratory determinations on ash from the same deposits, with values of U^*_{th} ranging from 0.13 to 0.38 m/s. Our results show that the median grain size of the deposit and particle shape have a stronger control on U^*_{th} than the local substratum nature and deposit texture.

1. Introduction

The resuspension of volcanic ash by wind following explosive eruptions is a well-known hazard (Arnalds et al., 2013; e.g., Hobbs et al., 1983; Miwa et al., 2018; Panebianco et al., 2017; Wilson et al., 2011). Besides the main control exerted by the local wind field, volcanic ash resuspension is also influenced by other factors, including: 1) atmospheric humidity; 2) features of the deposit (grain size distribution, particle morphology, sedimentary structures, etc.), and 3) features of the substrate (i.e., moisture, roughness) (De Vet et al., 2014; Del Bello et al., 2018; Douillet et al., 2014; Hadley et al., 2004; Liu et al., 2014; Miwa et al., 2018).

Volcanic ash resuspension is initiated when wind friction velocity overcomes the so called ‘threshold friction velocity’ U^*_{th} of a particle, detaching particles from a surface and emitting them into the atmosphere (Fécan et al., 1999; Greeley and Iversen, 1985; Iversen and White, 1982; Marticorena and Bergametti, 1995; Shao and Lu, 2000). Such parameter largely varies according to particle

microphysical properties, like e.g., size, sphericity, and porosity, making the U^*_{th} of volcanic particles, typically vesicular and irregular in shape, very different from that of, e.g., well rounded sand particles (e.g. De Vet et al., 2014).

U^*_{th} is a critical parameter to initialize numerical simulations that can forecast volcanic ash resuspension and dispersal in semi-real time during an eruption (Beckett et al., 2017; Folch et al., 2014; Hammond and Beckett, 2019; Leadbetter et al., 2012; Reckziegel et al., 2016), but that requires emission schemes that are calibrated for volcanic particles. So far, however, such models have relied on U^*_{th} parameterizations that are based on non-volcanic particles and often derived from idealized laboratory wind tunnel settings (i.e. Bagnold, 1941, Greeley and Iversen, 1985, Shao and Lu, 2000).

Measurements of U^*_{th} for volcanic ash have only been performed in the laboratory and for a limited number of test cases and environmental factors (Del Bello et al., 2018; Etyemezian et al., 2019; Fowler and Lopushinsky, 1986). In contrast, studies on wind transport in general and U^*_{th} measurements - particularly for soils and sand deposits - have largely benefited from direct measurements in the field, using portable wind-tunnels or other devices (Macpherson et al., 2008; Mejia et al., 2019; e.g., Nickling and Gillies, 1989; Pietersma et al., 1996; Sirjani et al., 2019; Sweeney et al., 2008; Van Pelt et al., 2010; Van Pelt and Zobeck, 2013). For volcanic ash, in-situ effects on U^*_{th} like e.g., textural features of the ash deposit, nature of the substrate onto which the ash is deposited (either natural or anthropic), soil and environmental humidity changes, have not been parameterized and potentially affect how particles are detached from the ground and resuspension is initiated. To this end, field measurements are crucial to study such natural factors and to capture their heterogeneity through time and across space.

In view of increasing the availability, accuracy, and precision of volcanic ash U^*_{th} measurements, and also in the perspective of quick response to future volcanic eruptions, we performed the first

field-based measurements of the U^*_{th} of volcanic ash by wind by developing and testing a small-scale, specifically designed, portable wind tunnel. The wind tunnel was calibrated in the laboratory and field tests were reproduced in the laboratory under controlled conditions.

2. Threshold friction velocity

U^*_{th} is typically studied within the framework of the particle saltation theory, where force balance models are used to quantify when wind-induced aerodynamic lift and drag forces exceed particles gravity and adhesion forces (e.g., Bagnold, 1941; Shao and Lu 2000, Merrison et al 2007). Based upon wind-tunnel experimental data where particle saltation threshold was measured (Greeley and Iversen, 1985; Iversen and Rasmussen 1999), Shao and Lu (2000) developed one semi-empirical force balance model to predict the size dependence of the threshold friction velocity using two empirical constants, one expressing the ratio between gravity and lift forces (A_n) and the other the ratio between adhesion and lift forces ($\gamma \cdot A_n$), i.e. $\boldsymbol{U^*_{th}} = \sqrt{\boldsymbol{A_n}\left(\frac{\boldsymbol{\rho_p g 2r}}{\boldsymbol{\rho_a}} + \frac{\boldsymbol{\gamma}}{\boldsymbol{\rho_a 2r}}\right)}$, where ρ_p and ρ_a are particle and air densities, g is gravity, r is the particle radius. The parameter values found for Terrestrial conditions using this model were $\boldsymbol{A_n}$= 0.0123 and $\boldsymbol{\gamma = 2.8 \div 3.6 \times 10^{-4}}$, for sand (Shao and Lu, 2000) and 'dry' volcanic particles (Del Bello et al., 2018). In another force balance model, developed to fit specific experimental data (Merrison et al. 2007, Merrison et al. 2012), the forces of adhesion ($\boldsymbol{F_{adh} = 2C_{adh}r}$), gravity ($\boldsymbol{F_g = \frac{4}{3}\pi g \rho_p r^3}$), fluid lift ($\boldsymbol{F_L = \rho U_*^2 C_L r^2}$) and a drag induced rotational force ($\boldsymbol{F_T = \rho U_*^2 C_T r^3}$) were separately incorporated, leading to: $\boldsymbol{U^*_{th}} = \sqrt{\frac{\frac{4}{3}\pi g \rho_p r^3 + 2C_{adh} r}{C_L r^2 + C_T r^3} \cdot \frac{1}{\rho_a}}$. Here, C_{adh}, C_L and C_T are the respective coefficients of adhesion, lift and effective size dependent torque coefficient. In the case of C_T = 0 the Shao and Lu (2000) and Merrison et al. (2012) models become entirely equivalent with conversion of the relevant coefficients

being $A_n = 2\pi/3C_L$, $\gamma = 6C_{adh}/\pi$. The Merrison et al. (2012) model, as opposed to other force balance models (e.g. Greeley and Iversen, 1985; Shao and Lu, 2000) allows the individual contribution of each acting force coefficient relating U^*_{th} to volcanic ash grain size to be empirically derived. Based upon previous wind tunnel detachment experiments, this model better reproduced experimental data for volcanic ash in a variety of humidity conditions, using parameter values of; $C_L = 160$, $C_T = 1.6 \times 10^6$ m^{-1} and C_{adh} varying from 1.8×10^{-4} to 1.1×10^{-3} N/m depending upon particle morphology (i.e. shape and porosity), and relative humidity (Del Bello et al., 2018).

Experimentally, the threshold friction velocity is determined from detecting initial saltation of particles (e.g. Iversen and White, 1982). The onset of particle transport through saltation is characterised by a first regime of discontinuous saltation flux – or bursting – where particles are released in intermittent bursts due to the turbulent wind velocity fluctuating around the so-called fluid, or static, threshold (Bagnold, 1941). When particles subsequently collide with the bed and eject other grains, a cascading response is triggered until particle flux becomes continuous and the dynamic threshold is reached (e.g., Carneiro et al. 2015).

3. Materials and Methods

3.1 Study cases

Two study areas were selected: freshly erupted volcanic ash from multiple Vulcanian explosions at Sakurajima volcano (Japan), settled in proximal areas, and a distal volcanic ash deposit from the 2011 Plinian eruption of Cordón Caulle volcano (Chile) (Fig. 1). Sakurajima volcano (hereafter SK), located in southern Japan, produces minutes-long explosions on a daily basis, with transient ash plumes 1 to 5 km high (Iguchi et al., 2013). The ash forms by fragmentation of a dense, largely crystallized andesitic magma plug (Iguchi et al., 2008), and the particles are mostly blocky in shape

and poorly vesicular (Miwa et al., 2013). This ash is continuously resuspended by winds, causing trouble to people living in the surrounding villages, and, depending on the wind strength and direction, carried over into the nearby city of Kagoshima (Poulidis et al., 2018).

The Puyehue-Cordón Caulle (hereafter CC) is a stratovolcano in the Southern Volcanic Zone of the Chilean Andes. A months-long eruption occurred at CC in 2011. In the first days of the eruption, the fragmentation of the rhyolitic magma generated vesicular volcanic ash that was injected up to 14 km-high into the atmosphere (Bonadonna et al., 2015). The ash, dispersed mostly eastward by the prevailing winds, settled over a large area of the Argentinean Patagonia (Panebianco et al., 2017), and, resuspended by wind, caused great economic and environmental damage through the following years (Craig et al., 2016; Forte et al., 2018).

All the tested ash beds were reworked deposits. The SK deposit was the result of ash accumulated over several days/weeks of volcanic activity whereas CC deposits were eight years old at the time of the experiments, and both have been repeatedly subjected to wind erosion and transport, and rain events.

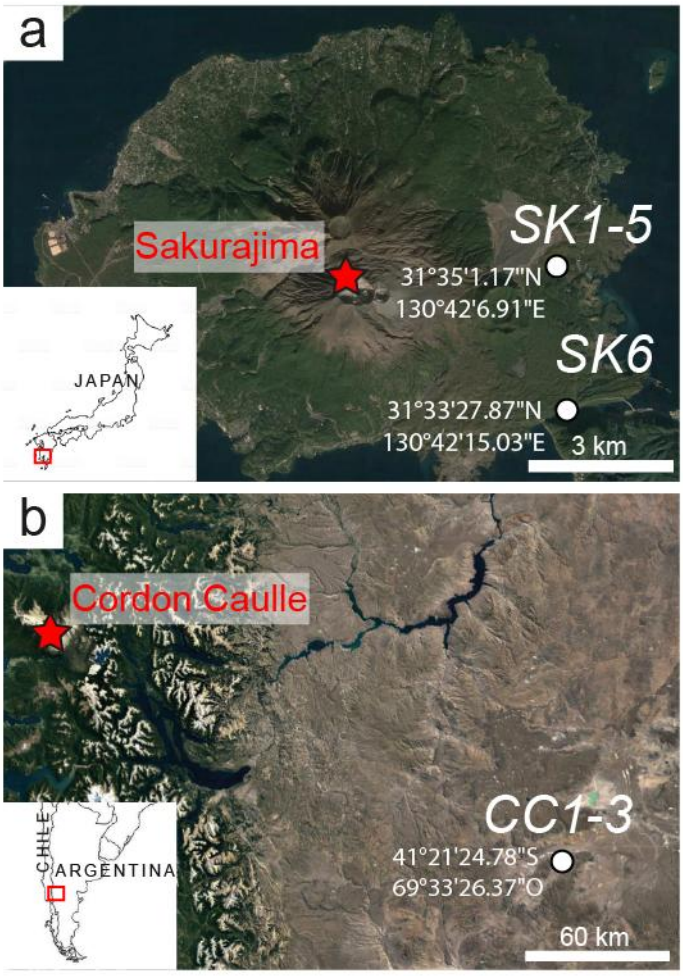

Figure 1. (a-b) Location (white dots and associated run names) and source volcanoes (red stars) of the test case volcanic ash deposits. SK test sites are located at 3-5 km from the source, an active vent of Sakurajima volcano (Japan), whereas CC one is located in the Patagonian Steppe (Argentina), 250 km away from the Puyehue-Cordón Caulle stratovolcano (Chile)

3.2 Experimental setup and runs

The Portable Wind tunnel for Ash Resuspension (PoWAR) is a custom-designed, small wind tunnel that generates a controlled wind flow within a 110x12x12 cm transparent test section open at the base, which can be placed directly on an ash test bed. PoWAR is conceived as a simple, low-budget prototype made of off-the-shelf materials. The Plexiglas ® test section is preceded by a cardboard

inlet (also open at the base), and followed by a cardboard junction, in turn, connected to the airflow generator, a commercial leaf blower (Dream Power ® EB-26D) set in suction mode. Attached to the airflow outlet there is an ash sampler, i.e., a plastic cylinder with a funnel bottom and a collecting vial (Fig. 2). Wind speed is measured by a hot wire anemometer (PCE ® 423, precision ± 5% of reading, 1 Hz sampling rate) at the down-flow end of the test section and 5 mm above the testbed. Particle motion is documented using up to two high-speed (HS) cameras (Optronis ® CR600x2 and NAC ® HX6) and two high-definition (HD) camcorders (Sony ® FDR-AX 100E). The high-speed cameras recorded particles motion at high spatial (25 µm per pixel) and temporal (2000 frames per second) scales, either from the side or from the top of the transparent test section. The camcorders recorded at 60 frames per second, capturing images of the particles either at the wind tunnel inlet or from the top (Fig.2, Fig. 3a and e).

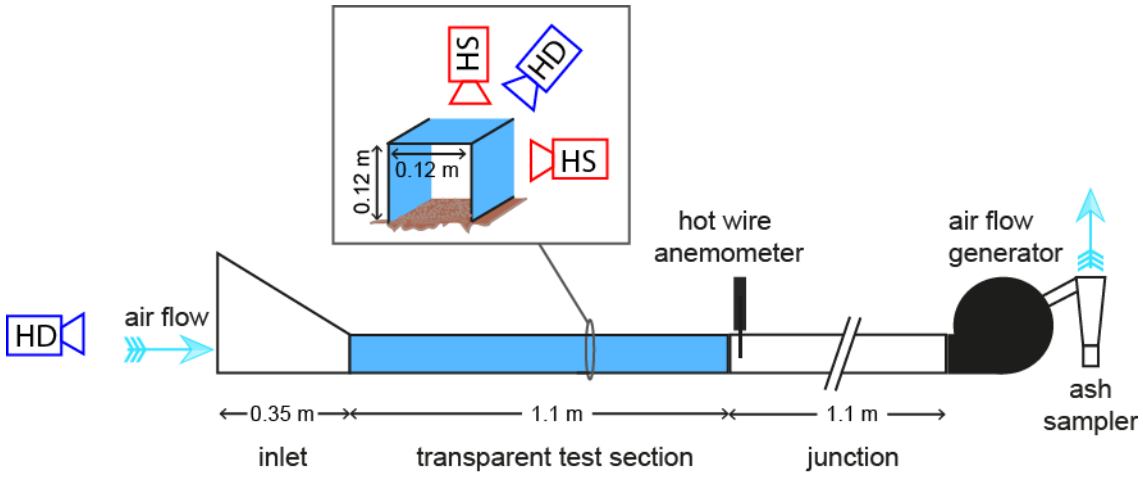

Figure 2. (a) Sketch of the experimental apparatus and location of the high-definition (HD) and high-speed cameras (HS).

To measure U^*_{th}, ramp-up experiments were performed by increasing the wind speed stepwise over time from a minimum of 1 m/s to a maximum of 6-9 m/s (with 2 cases up to 12.5 m/s). Step height and duration was 0.5 m/s and 2 minutes, respectively. During each experiment, lasting ca. 20-25

minutes, wind velocity and HD videos were recorded continuously, and one (0.55 s long) HS video was recorded in the middle of each wind step. Resuspended ash was collected at every step for 1 minute in a vial that was replaced between each step. It must be noted that this sampling methodology only allowed to collect the coarser particles of the resuspended material, the finest portion (roughly lower than ~30 μm) being transported and dispersed out by the airflow. For each step: 1) the average wind velocity (and its standard deviation) was calculated over the 2 minutes-long wind step window, 2) the mass of ash particles collected by the sampler was obtained by weighing, and proxies for the amount of moving particles were quantified from video analysis. For SK, the number of moving particles was estimated automatically for each frame of the HS videos after image subtraction and image thresholding, via the 'analyse particles' routine of the ImageJ freeware (Schneider, C. A., 2012) (see Video 1 for an example of HS video and particles count), and the cumulative number computed over 1000 frames. For CC, particle automatic detection was not possible due to the low contrast between CC rhyolitic ash particles and the background, so instead, HD videos were used. Grey tone changes were analysed within a region of interest by using the 'measure' routine of ImageJ (see Video 2 for an example of HD video and grey tone measurement), and the average grey tone value computed over the ca. 2000 consecutive frames corresponding to each wind speed step. Sampled mass, particle count, and grey tone measurements are well reproducible within each experiment and are used only to identify the onset of U^*_{th}. During all experiments, environmental conditions, i.e., ambient temperature, humidity and wind speed and direction, were constantly recorded using a HOBO ® weather station at 1.5 m above the ground.

166 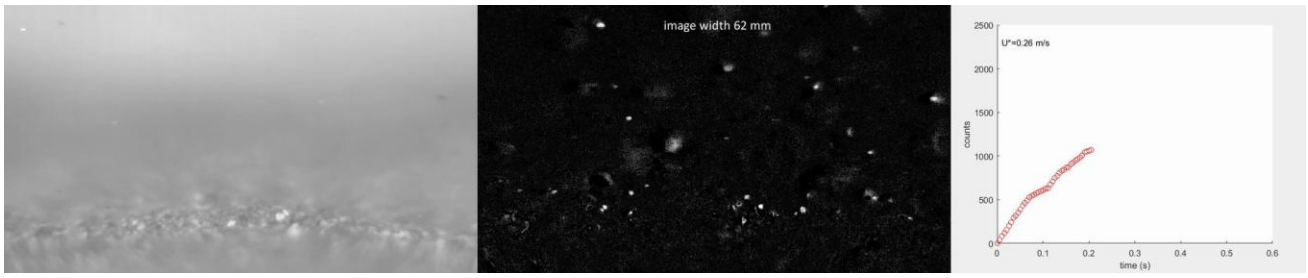

167 Video 1: Determination of the resuspension threshold friction velocity by high-speed imaging. The video is a
168 montage of three short video sequences, each 0.55 s long, at three steps of increasing U^* (0.22, 0.24, and 0.26
169 ms^{-1}) during run SK6. The left-hand panel shows the original high-speed video (image width is 62 mm), while
170 the central panel shows the same video after image subtraction (mathematical subtraction of pixel values of
171 one frame from the subsequent one, effectively removing the static background). In the right-hand panel, the
172 cumulative number of particles counted in the image subtraction video over time, after arbitrarily setting a
173 grey level threshold and a minimum number of pixel per particles. The sharp increase in the number of
174 resuspended particles for increasing U^* is evident.

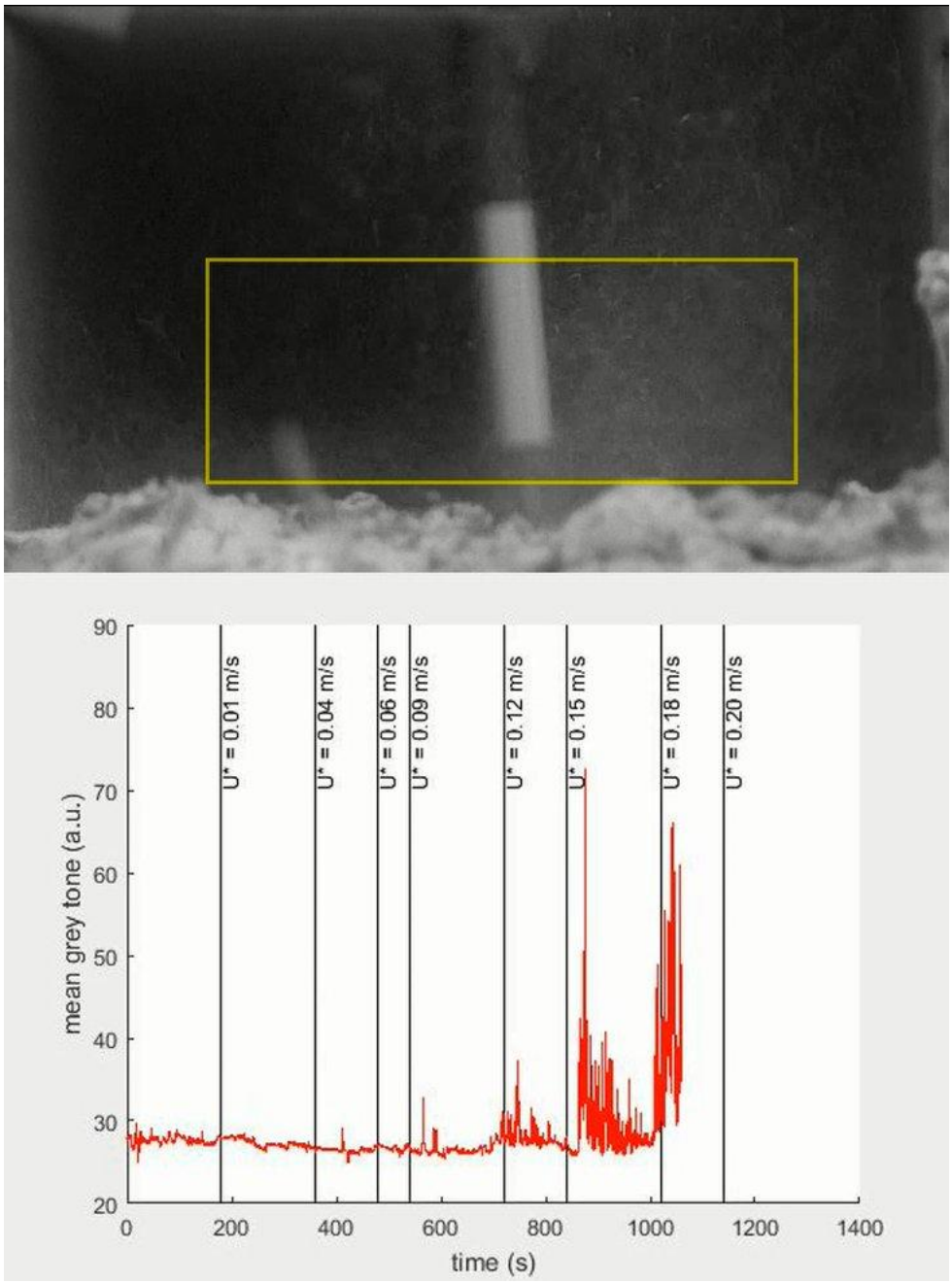

Video 2: Determination of the resuspension threshold friction velocity by high-definition imaging. The video covers the whole duration of experiment CC1 and is shown at 50 times the original speed. In the upper panel, the frontal view into PoWAR by high-definition video, showing the test bed (bottom, in the foreground) and the hot wire anemometer (7 mm across for scale, in the background). In yellow, the region of interest over which the mean grey tone is measured. In the bottom panel, changes in the mean grey tone over time. The vertical lines mark the time when U^* was increased to the corresponding step value.

The SK experiments were performed in January 2019 at two localities at about 3 and 5 km from the active vent. At the Kurokami branch of the Sakurajima Volcano Research Center, we performed runs SK1-3 consecutively on the same testbed, i.e., the ash-covered (thickness ca.1 cm) concrete parking lot, and runs SK 4 and 5 on two different grass-free land patches. At a parking lot between two local roads, we performed run SK6 on the asphalt covered by an ash layer (thickness ca. 1 cm, Fig 3a-b) with a ripple-like surface (Fig. 3c-d). Environmental conditions during the experiments were air temperature 10-14 °C, relative humidity (RH) 44-51%, wind speed 0.7-1.7 m/s.

The CC experiments were performed in October 2019 around the city of Ingeniero Jacobacci in the Patagonian steppe of Argentina and about 250 km from the source volcano. There, the CC ash is present as meters-large, 3-5 centimeters thick patches mostly surrounded by sparse vegetation. CC1-3 experiments were run consecutively on the same testbed, i.e., ash (thickness ca. 5 cm, Fig. 3e-f) covering a small, flat land patch. Environmental conditions during the experiments were air temperature 13-15 °C, and RH 22-23%, with no appreciable wind.

Two laboratory resuspension experiments were performed at the Aarhus University Wind Tunnel Simulator II (AWTSII) using unsieved SK ash samples and following the experimental procedure of Del Bello et al. (2018), using 5% and 83-96 % RH ambient humidity, respectively. These controlled experiments (ramp-up, with 2 min width and 0.5 m/s height wind speed steps) investigated: i) the effect of ambient humidity on the U^*_{th}, and ii) any possible resuspension difference between an artificially prepared, homogeneously thick ash layer (5 mm) and the ash beds in the field, i.e. subject to natural reworking processes. We also repeated a field SK experiment using PoWAR in the laboratory, on an ash sample collected before the SK-6 run and artificially prepared with a scraper into a homogeneously thick (3 mm) layer .

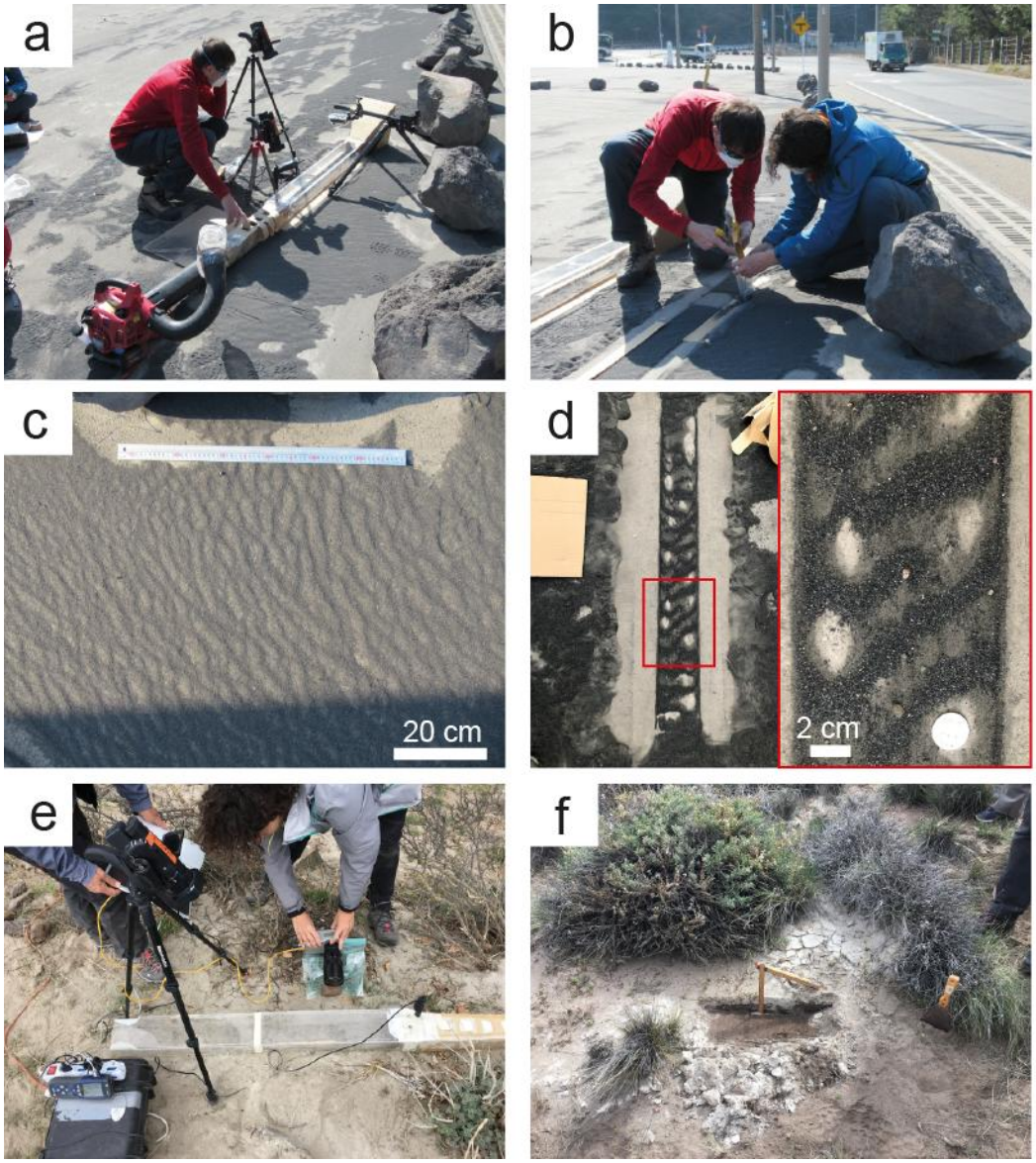

Figure 3. Experimental procedure and ash sampling. (a-b) Apparatus deployment and post-test sampling of ash from the testbed after run SK6. (c-d) Example of an undisturbed pre-experiment and post-experiment testbed (run SK6), zoomed in the red inset. (e-f) Apparatus deployment before run CC1-3 and sampling of the CC ash near the CC1-3 site. Volcanic ash is the light tan patch near vegetation. Vertical ruler for scale (20 cm).

3.3 Setup calibration

PoWAR was calibrated at AWTSII using three independent methods to characterize airflow development as a function of airspeed as measured by the hot wire anemometer (Fig. 4). First, with

PoWAR deployed as in the field, a Laser Doppler Anemometer (LDA, DANTEC ®) was used to measure the horizontal and vertical component of the wind speed along the centreline of the test section and 2 cm above the base, at different positions along the test section (15, 40, 60, 80 and 105 cm from inlet side). In this case, the basal surface used for the calibration was glued with 200 µm sized sand particles. LDA measurements were converted to shear velocity, U^* as per Del Bello et al. (2018). Secondly, using a Pitot tube the average horizontal velocity was measured in the test section over a sand and an ash bed at elevations of 3.5, 6, 9, 15 and 25 mm, and in the same position as the anemometer. This is within the zone where the turbulent boundary layer with constant bed shear stress has a log-linear segment (The Law of the Wall, White, 1991). This allowed U^* to be calculated from a log-linear fit to the measured velocities and von Karman's constant (k=0.4). Thirdly, in the laboratory, POWAR was applied (as in the field) on four different sand beds each composed of uniform samples (average particle diameters 125, 170, 240, 320 µm, respectively) having known U^*_{th} (Iversen and Rasmussen, 1994). For each bed the hot-wire signal was measured at saltation threshold. It should be noted that in two field experiments (SK5-6) the range of friction velocities exceeded the range used in the calibration (U^* > 0.33 m/s), and therefore, in this case, an extrapolation of the calibration curve has been made.

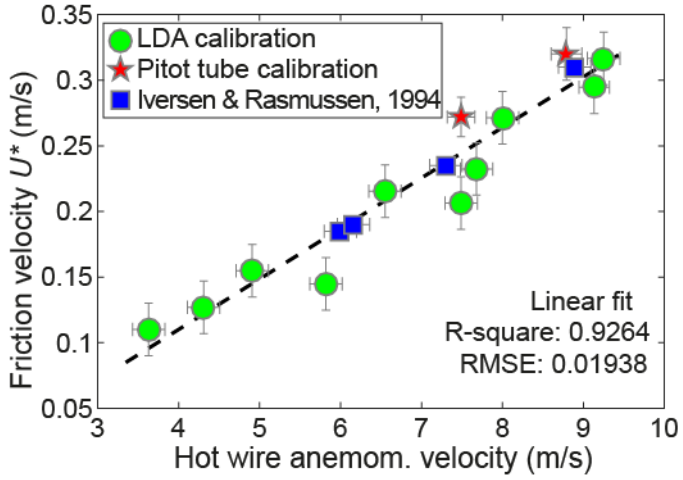

Figure 4. Portable wind tunnel calibration. Relationship between the wind speed in the wind tunnel, measured by hot wire anemometer, and friction velocity (U^*), obtained by i) Laser Doppler Anemometry, ii) Pitot tube profiling of the vertical wind flow, iii) U^*_{th} measurements of well-characterized sand material (Iversen and Rasmussen, 1994). Error bars are the standard deviation of the measured wind speed over the run duration (X-axis) and the measurement variance of LDA and Pitot tube measurements (Y-axis).

3.4 Ash samples characterization

Ash samples were collected before, during, and after the experiments. Pre- and post-experiment samples were collected at the side of the testbed and from it, respectively (Fig. 3b, c). Ash particle morphology was characterized under a Field Emission Scanning Electron Microscope (FESEM, JEOL ® JSM 6500F) at INGV Roma, and particle size distribution of the samples was determined by laser diffraction granulometry (MALVERN ® 2000) at the Dept. of Science of the Università Roma Tre (Fig. 5).

4. Results

SK particles are mostly non-vesicular to poorly vesicular and blocky in shape, including a relatively large proportion of loose crystals. CC particles are largely vesicular, of ragged and irregular shape, and almost entirely composed of glass shards with very few loose crystals. The particle size distribution (PSD) of SK samples is relatively broad and strongly skewed towards the coarse fraction¸ while the PSD of CC samples is less skewed, much finer and better sorted. In all cases except one (SK5), the post-experiment samples tend to be depleted for particles in the size range 100-500 µm relative to the pre-experiment ones.

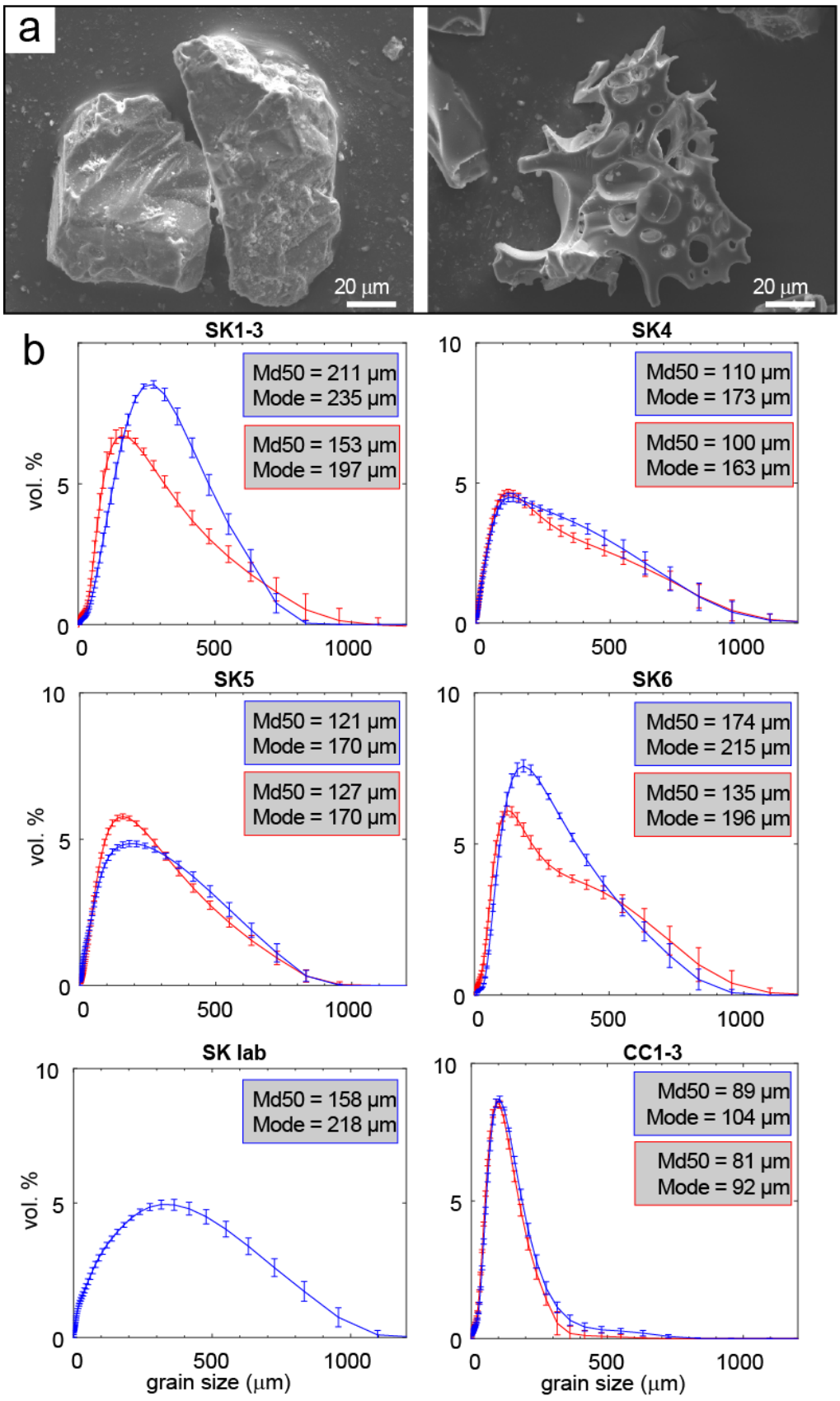
a
20 µm
20 µm
b
SK1-3
Md50 = 211 µm
Mode = 235 µm
Md50 = 153 µm
Mode = 197 µm
SK4
Md50 = 110 µm
Mode = 173 µm
Md50 = 100 µm
Mode = 163 µm
SK5
Md50 = 121 µm
Mode = 170 µm
Md50 = 127 µm
Mode = 170 µm
SK6
Md50 = 174 µm
Mode = 215 µm
Md50 = 135 µm
Mode = 196 µm
SK lab
Md50 = 158 µm
Mode = 218 µm
CC1-3
Md50 = 89 µm
Mode = 104 µm
Md50 = 81 µm
Mode = 92 µm
vol. %
grain size (µm)
0
5
10
500
1000

Figure 5. Morphology and grain size distribution of ash samples. (a) FESEM images of representative ash particles from the SK and CC samples (left-hand and right-hand pictures, respectively). (b) Grain size distribution of the pre- (blue) and post- (red) experiment ash deposits. Each curve is the average of 30 measurements, with the standard deviation in the error bars. Median (Md50) and modal values are also reported. Note that in the SK lab case, a post-experiment residual sample was not available due to total sample removal.

The different methods used to detect particle detachments, i.e., video analysis and ash sampling, provided closely matching results (Fig. 6). In both SK and CC datasets, ash deposits with a coarser PSD show steeper curves, departing from zero at the lowest U^* values in the two datasets. As the median grain size of the deposit decreases, the curve starts to depart from zero at higher shear velocities, i.e. at higher U^* values.

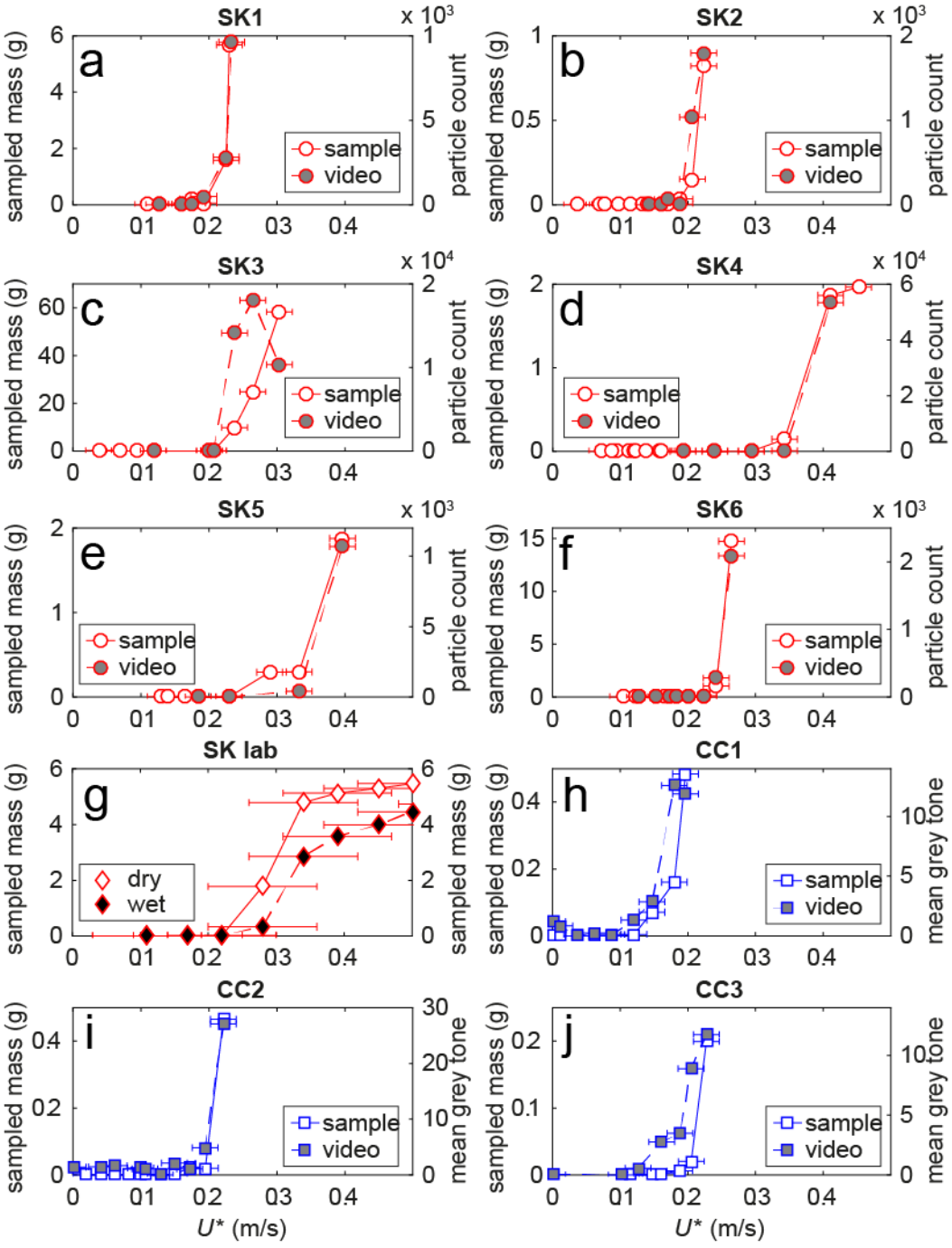

Figure 6. Results from field and laboratory *U** ramp up tests. In each panel, different proxies for the amount of resuspended particles are plotted against the mean *U**. (a-f) SK field experiments: sampled mass of resuspended ash collected in the ash sampler (white filled symbols), and number of resuspended particles crossing the field of view of the high-speed camera (grey filled symbols). (g) SK laboratory experiments: removed mass measured in dry (5 % RH, white filled symbols) and wet (83-96 % RH, black-filled symbols)

267 environmental conditions. (h-j) CC field experiments: sampled mass (white symbols) and mean gray tone of
268 the high definition camera video (after background subtraction). Note variable vertical axes scale. Horizontal
269 bars are RMSE of the wind-speed-friction velocity calibration fit curves (0.02 m/s for field data and 0.08 m/s
270 for lab data).

271 In all methods, the threshold friction velocity U^*_{th} was visually determined to have occurred where
272 the *y*-axis value of the data in Fig. 6 start to significantly depart from zero. The mean U^*_{th} is
273 calculated taking the minimum and maximum U^* values corresponding to the mean friction velocity
274 of the wind steps preceding and following the threshold, respectively (Fig. 7a). The identified
275 thresholds are confirmed from visual observation during the experiments, where the same U^*
276 intervals corresponded to the transition from intermittent to sustained bursting (Carneiro et al. 2015).
277 For Cordón Caulle, U^*_{th} values calculated from the sampled mass of CC 1-3 show a clear increase in
278 mean U^*_{th} with progressive run number, however, the values obtained from the greyscale analysis do
279 not match in run CC3, showing a drop in mean U^*_{th}. For Sakurajima, the SK2 run exhibits a smaller
280 mean U^*_{th} (but within min and max U^*_{th} range) than SK1, whilst run SK3 shows a clearly higher
281 mean U^*_{th}, value (Figure 7a).

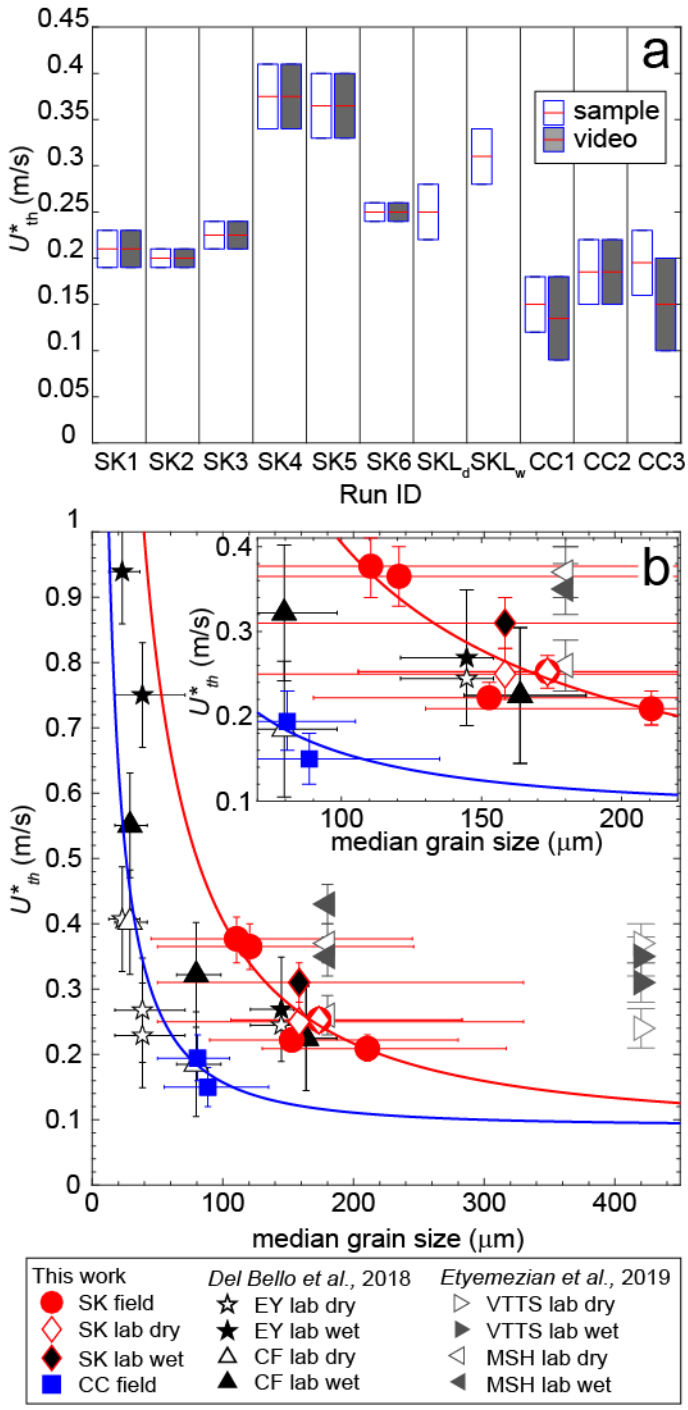

Figure 7. U^*_{th} values for Sakurajima and Cordón Caulle ash. (a) U^*_{th} for each run as obtained from sampled mass (white boxes) and video analysis (grey boxes). Note that Runs SK 1-3 and CC1-3 are for three consecutive runs on the same testbed. Threshold is identified visually from the curve segments in Fig 6 were the *y*-axis value of the data significantly depart from zero. The boxes comprise the lower and upper U^*_{th} values

(box height, corresponding to min and max U^* of the curve segment, and the mean U^*_{th} value (red line). (b) U^*_{th} (obtained from sample mass) as a function of the median grain size distribution of our field experimental data (SK field and CC field), compared with our laboratory determinations (SK lab) and literature values (Del Bello et al. (2018) and Etyemezian et al. (2019)). Horizontal and vertical error bars are the 25^{th}-75^{th} percentiles of the grain size distribution and the RMSE of the calibration fit curve (Fig. 4), respectively. Lines are force balance equation fits (Merrison et al., 2007) to SK (red) and CC (blue) ash deposits considering three fitting parameters (see text). Inset shows closer view of the central part of (b). Runs SK2 and CC2 are not shown, as no grain size data were collected in the middle of the repeated runs on the same testbed.

Mean U^*_{th} values for CC data, in the range 0.13-0.19 m/s for median diameter values of 89-81 μm, are remarkably lower than SK ones, ranging from 0.19 to 0.38 m/s for median diameter values 211-110 μm. Comparing field results with laboratory experiments on the SK ash provide constraints in terms of humidity effects (Fig. 7). In particular, the laboratory experiments performed at dry condition (5% RH) both in the environmental chamber and in PoWAR provided mean U^*_{th} of 0.25 ± 0.03 m/s, matching well the field derived values with similar median size at RH conditions of 45-50%. Conversely, for the same median grain size, the environmental chamber experiment at RH 83-96 % provided a higher value of mean U^*_{th} (0.31 m/s).

Our field-based data are compared with published laboratory determinations from Del Bello et al. (2018) and Etyemezian et al. (2019), on volcanic ash from the following eruptions: Eyjafjallajökull, 2010 (EY, Iceland); Campi Flegrei Pomici Principali Layer A, 10 ka (CF, Italy), Novarupta, 1912 (VTTS, USA), and Mount St. Helens, 1980 (MSH, USA). For all these literature data, we report data for dry (RH < 16%) and wet (RH> 82%) experimental conditions (Fig. 7b). We applied to our data the force balance model of Merrison et al. (2007, see section 2) to model the U^*_{th} dependence on median grain size. We considered a particle density ρ_p =2400 kg/m^3 (Suh et al., 2019) and 1400 kg/m^3 (Pistolesi et al., 2014) for SK and CC field data respectively, and applied a nonlinear least-

311 squares method using Matlab Curve fitting toolbox, imposing non-negativity bounds on the three
312 fitting parameters (C_{adh}, C_L, and C_T). In this case the Merrison model provided the best fit to the
313 observed SK and CC data (R^2 0.79 and 0.42, respectively), and the resulting values of the fitting
314 parameters were C_{adh}= 2.4 x10^{-3} N/m and 2.5 x10^{-4} N/m, C_T =1.0 × 10^7 m^{-1} and 9.9 × 10^6 m^{-1},
315 respectively. When C_{adh} is considered as the fitting parameter, and the two other coefficients are
316 assumed constant (C_L = 160 C_T = 1.6 × 10^6 m^{-1}, as per other volcanic particles, Del Bello et al.,
317 2018), a poorer fit is obtained (R^2 0.53 and 0.11, respectively) and the resulting values of the fitting
318 parameters are C_{adh}= 7.4 x10^{-4} N/m and 9.7 x10^{-5} N/m for SK and CC, respectively. Overall, all data
319 follow a common trend of decreasing U^*_{th} with increasing median size. Wet conditions always result
320 in higher U^*_{th} with respect to dry ones, more markedly for the smaller grain sizes. Ash samples from
321 individual eruptions display clear specificities. The 'dry' EY and CF ash experimental data align on
322 the modelling fit for CC data. Conversely, the 'wet' EY and CF ash experimental data are placed
323 within the SK and CC modelling fits. VTTS and MHS ash data are not described by any of the two
324 modelling curves.

325 **5. Discussions**

326 5.1 The variability of threshold friction velocity of volcanic ash

327 A noticeable difference appears in the field-measured U^*_{th} values of CC and SK ash deposits, the
328 former being more easily remobilized by wind. Factors that may explain this difference include
329 variations in i) the grain size distribution of the two deposits, ii) particle morphology and vesicularity,
330 and iii) texture and substratum of the ash deposits.

331 Concerning the grain size distribution, the larger range of U^*_{th} values measured for SK with respect
332 to CC is consistent with the broader range of median particle diameter of the different testbeds of SK.

However, differences in the median diameter fails to explain the differences between CC and SK. In fact, the finest SK and the coarsest CC samples have similar median particle diameter (~100 μm) but the former has a higher U^*_{th}. The former ash is also significantly less sorted than the latter (Fig. 5 and horizontal error bars in Fig. 7), but this cannot explain the different U^*_{th}. In fact, poorer sorting should result in larger availability of larger particles and thus in lower U^*_{th} (see below).

Vesicularity plays a central role in the lower U^*_{th} of CC with respect to SK ash particles, the former being highly vesicular and of irregular shape, the latter being an extreme case - in volcanic products - of low- to non-vesicular particles of blocky shape. In the CC case, high vesicularity implies a low bulk density, reducing the gravitational force, and a very irregular particle shape (Fig. 5a), which decreases the effective contact radius and thus adhesion force (Goldasteh et al., 2012; Johnson et al., 1971). A parametric analysis using the force balance model shows that density differences between SK and CC cause a negligible change in U^*_{th}, while the shape-related adhesion coefficient, one order of magnitude lower in CC relative to SK samples, is the dominant factor explaining the remobilization of CC ash at such low friction velocities.

Textures and substratum of the ash deposits do not seem to play a crucial role in controlling U^*_{th}. Runs performed on paved surfaces covered with ripple-like ash beds (SK1-3, Fig. 3e) do not show significant variations from runs performed on ash-covered soils (SK 4-5), both groups not deviating significantly from the size-dependent trend predicted by the force balance model (Fig. 7). Furthermore, the deviation of the data points from the model is within the range established by varying humidity during laboratory determinations of U^*_{th} on the same SK ash samples, suggesting that substratum nature and deposit structure contribute only secondarily to influencing resupension threshold.

The results of our field experiments are in line with previous laboratory determinations of U^*_{th} (Fig.

7). The SK ash field experiments highlight the control of the grain size distribution on U^*_{th} in the investigated size range, and lie on the upper end range of the behaviour of EY and CF ash samples in wet laboratory conditions (Del Bello et al., 2018). The CC ash model curve reveals that CC, EY and CF ash samples in dry laboratory conditions follow a common trend. CC ash samples display the lowest U^*_{th} ever measured so far for volcanic sediments, as a result of their very irregular particle morphology. However, it should be noted that the measured value is within the uncertainty of the corresponding value of Campi Flegrei in dry conditions. This very low U^*_{th} contributed to exacerbate the effects of wind resuspension in the Argentinean Patagonia after the CC eruption (Dominguez et al., 2020).

5.2 Threshold friction velocity and ash deposit evolution over time

With the exception of SK5, after all experiments, we observed depletion of the ash deposits for particles in the size range ca. 100 - 500 µm, with SK1-3 and SK6 residual samples showing clear relative enhancement of particle fractions greater than 500-600 µm. We also observed, at least in the CC sampled mass case, a shifting of U^*_{th} to higher values when runs were repeated on the same testbed. We interpret this as being a result of the easier removal of coarse particles. As predicted by the force balance model, and assuming spherical particles and constant density, particles with larger diameter are more prone to be detached due to their gravity force and aerodynamic drag dominating over cohesive force and aerodynamic lift (see Merrison, 2012 for a review). Furthermore, larger particles likely protruded from the undisturbed test bed, thus triggering bursting events and favouring early resuspension (i.e., at low U^*_{th}) in the very first runs. The increase of U^*_{th} over repeated runs on the same testbed was also observed in the laboratory by Etyemezian et al. (2019), and attributed to the removal, in the first run, of 'most readily suspendable material' resulting from artificial testbed preparation. Since our field experiments were performed on natural surfaces, increasing U^*_{th} over

repeated wind erosion events may be a natural evolution in ash deposits. Our field testbeds have been subjected to complex reworking by wind and water for a time span variable from days-weeks at SK and to years at CC. In particular, at the SK6 site, we witnessed wind-induced ash resuspension and ash-devils during our field campaign, the ash cover in the parking lot shifting its position from day to day. Wind resuspension is likely to act on dominantly reworked deposits even in the immediate aftermath of an eruption, as the top surface of any deposit is often affected by wind and water even during eruptions, as a function of local climate and depositional rates from the eruption plume (Dominguez et al., 2020; Forte et al., 2018; Thorsteinsson et al., 2012).

5.3 Field vs. laboratory resuspension experiments

Field measurements of U^*_{th} have several advantages over laboratory ones, such as investigating the effect of local factors, e.g., small-scale variations in grain size distribution and textural features of the deposits, local environmental conditions, and the presence of small-scale vegetation and slope. Recently, field-based measurements have been performed for dust emission studies of sand dunes, using a portable device that estimates both the U^*_{th} and the emissivity, i.e. the removed mass of soil per unit surface and time (Mejia et al., 2019; Sweeney et al., 2008). In our study, we solely focused on U^*_{th} measurements and not on emissivity, that is also important for hazard assessment in the case of volcanic ash resuspension (Etyemezian et al., 2019). U^*_{th} data from PoWAR could be used within existing empirical models to predict emissivity values once specific deposit characteristics are known (e.g., Gillette and Passi, 1988; Etyemezian et al., 2019), or, in the future PoWAR could be combined with a PM10 detector to directly measure the emissivity dependence upon U^* in the field. The transparent test section of PoWAR gives visual access to the detachment dynamics. Although not reported here, our high-speed cameras filmed, in nature, the fine details of particle motion in 3-D, including rocking, rolling, detachment, splash, saltation, and ripple-like structure formation. Finally,

PoWAR measurements are relatively fast, taking about an half-hour including setup, without the use of electrical power. The use of a commercial camcorder or even a simple ash sampler is shown to effectively determine U^*_{th} (Fig. 6), making PoWAR a rather inexpensive but effective apparatus. Calibration remains the most demanding task but needs to be performed only once.

The study we performed is the first attempt to parameterize the wind-induced resuspension threshold of volcanic ash directly in the field, in two very different areas heavily affected by wind-induced ash resuspension. The PoWAR proved to be a well-calibrated, inexpensive and yet effective tool that can expand our ability to investigate resuspension processes. Within the limited number of sites tested in this pioneering study, it appears that, in nature, the median grain size of the deposit and the differences in particle shape have a first-order control that can mask second-order effects induced by local substratum and deposit textures.

Conclusions

This study provides the first systematic attempt to parameterize how naturally reworked ash can be resuspended by wind. Our calibrated small, portable wind tunnel provided an easy and efficient way to quantify the threshold friction speed for initiation of volcanic ash particle motion, directly in the field. Our field-based measurements agree well with measurements performed in the laboratory, showing the interchangeability of field-and laboratory-based measurements. We also show that ash layers from different eruptions are resuspended differently by wind, depending less on the heterogeneity of the deposit and the variability of the substratum on which they rest and more on the size, density, and shape of the particles.

Declaration of competing interest

The authors declare that there no competing interest associated with this study.

CRediT author statement

EDB**:** Conceptualization, Methodology, investigation, Data Curation, Writing-Original draft. JT: Conceptualization, Methodology, investigation, Data Curation, Writing-Original draft. JPM: Methodology, Resources, Investigation, Review and Editing. KRR*:* Methodology, Resources, Investigation, Review and Editing. DA: Investigation, resources, funding acquisition. TR**:** investigation, resources. PS: Investigation, Resources, Supervision, funding acquisition. JJI: Resources, Methodology.

Acknowledgments

We acknowledge A. Vona and F. Basile (Roma Tre) for grain size analyses, A. M. Gaetano (INTA), T. Miwa, and T. Yamada (SVRC) for field support and kindness, C. Bonadonna for workshop 'Resuspension of Volcanic Ash' organization. Funding provided by MIUR Premiale 2015 Ash-RESILIENCE, and EUROVOLC Project ID: 731070, under H2020-EU.1.4.1.2. – Integrating and opening existing national and regional research infrastructures of European interest.

References

Arnalds, O., Thorarinsdottir, E.F., Thorsson, J., Waldhauserova, P.D., Agustsdottir, A.M., 2013. An extreme wind erosion event of the fresh Eyjafjallajökull 2010 volcanic ash. Sci. Rep. https://doi.org/10.1038/srep01257

Bagnold, R.A., 1941. The Physics ofBlown Sand and Desert Dunes. Methuen, London, pp. 265

Beckett, F., Kylling, A., Sigurardóttir, G., Von Löwis, S., Witham, C., 2017. Quantifying the mass

445 loading of particles in an ash cloud remobilized from tephra deposits on Iceland. Atmos. Chem.
446 Phys. 17, 4401–4418. https://doi.org/10.5194/acp-17-4401-2017

447 Bonadonna, C., Cioni, R., Pistolesi, M., Elissondo, M., Baumann, V., 2015. Sedimentation of long-
448 lasting wind-affected volcanic plumes: The example of the 2011 rhyolitic Cordón Caulle
449 eruption, Chile. Bull. Volcanol. 77. https://doi.org/10.1007/s00445-015-0900-8

450 Carneiro, M. V., Rasmussen, K.R., Herrmann, H.J., 2015. Bursts in discontinuous aeolian saltation.
451 Sci. Rep. 5, 1–8. https://doi.org/10.1038/srep11109

452 Craig, H., Wilson, T., Stewart, C., Outes, V., Villarosa, G., Baxter, P., 2016. Impacts to agriculture
453 and critical infrastructure in Argentina after ashfall from the 2011 eruption of the Cordón Caulle
454 volcanic complex : an assessment of published damage and function thresholds. J. Appl.
455 Volcanol. https://doi.org/10.1186/s13617-016-0046-1

456 De Vet, S.J., Merrison, J.P., Mittelmeijer-Hazeleger, M.C., Van Loon, E.E., Cammeraat, L.H., 2014.
457 Effects of rolling on wind-induced detachment thresholds of volcanic glass on Mars. Planet.
458 Space Sci. 103, 205–218. https://doi.org/10.1016/j.pss.2014.07.012

459 Del Bello, E., Taddeucci, J., Merrison, J.P., Alois, S., Iversen, J.J., Scarlato, P., 2018. Experimental
460 simulations of volcanic ash resuspension by wind under the effects of atmospheric humidity.
461 Sci. Rep. 8, 1–11. https://doi.org/10.1038/s41598-018-32807-2

462 Dominguez, L., Bonadonna, C., Forte, P., Jarvis, P.A., Cioni, R., Mingari, L., Bran, D., Panebianco,
463 J.E., 2020. Aeolian Remobilisation of the 2011-Cordón Caulle Tephra-Fallout Deposit :
464 Example of an Important Process in the Life Cycle of Volcanic Ash 7, 1–20.
465 https://doi.org/10.3389/feart.2019.00343

Douillet, G.A., Rasmussen, K.R., Kueppers, U., Lo Castro, D., Merrison, J.P., Iversen, J.J., Dingwell, D.B., 2014. Saltation threshold for pyroclasts at various bedslopes: Wind tunnel measurements. J. Volcanol. Geotherm. Res. 278–279, 14–24. https://doi.org/10.1016/j.jvolgeores.2014.03.011

Etyemezian, V., Gillies, J.A., Mastin, L.G., Crawford, A., Hasson, R., Van Eaton, A.R., Nikolich, G., 2019. Laboratory experiments of volcanic ash resuspension by wind. J. Geophys. Res. Atmos. 124, 1–27. https://doi.org/10.1029/2018JD030076

Fécan, F., Marticorena, B., Bergametti, G., 1999. Parameterization of the increase of the aeolian erosion threshold wind friction velocity due to soil moisture for arid and semi-arid areas. Ann. Geophys. 17, 149. https://doi.org/10.1007/s005850050744

Folch, A., Mingari, L., Osores, M.S., Collini, E., 2014. Modeling volcanic ash resuspension - Application to the 14-18 October 2011 outbreak episode in central Patagonia, Argentina. Nat. Hazards Earth Syst. Sci. 14, 119–133. https://doi.org/10.5194/nhess-14-119-2014

Forte, P., Domínguez, L., Bonadonna, C., Gregg, C.E., Bran, D., Bird, D., Castro, J.M., 2018. Ash resuspension related to the 2011 – 2012 Cordón Caulle eruption , Chile , in a rural community of Patagonia , Argentina. J. Volcanol. Geotherm. Res. 350, 18–32. https://doi.org/https://doi.org/10.1016/j.jvolgeores.2017.11.021

Fowler, W.B., Lopushinsky, W., 1986. Wind-blown volcanic ash in forest and agricultural locations as related to meteorological conditions. Atmos. Environ. 20, 421–425. https://doi.org/10.1016/0004-6981(86)90081-8

Gillette, D.A., Passi, R., 1988. Modeling dust emission caused by wind erosion. J. Geophys. Res. 93, 14233–14242. https://doi.org/10.1029/jd093id11p14233

Goldasteh, I., Ahmadi, G., Ferro, A., 2012. A model for removal of compact, rough, irregularly shaped particles from surfaces in turbulent flows. J. Adhes. 88, 766–786. https://doi.org/10.1080/00218464.2012.694278

Greeley, R., Iversen, J. D., 1985. Physics of particle motion, in: Cambridge university (Ed.), Wind as a Geological Process on Earth, Mars, Venus and Titan. pp. 67–104.

Hadley, D., Hufford, G.L., Simpson, J.J., 2004. Relic volcanic ash and dust still an aviation hazard. Bull. Am. Meteorol. Soc. 85, 1648–1649. https://doi.org/10.1175/1520-0434(2004)019<0829:RORVAA>2.0.CO;2

Hammond, K., Beckett, F., 2019. Forecasting resuspended ash clouds in Iceland at the London VAAC. Weather 74, 167–171. https://doi.org/10.1002/wea.3398

Hobbs, V., Hegg, D.A., Radke, L.F., 1983. Resuspension of volcanic vsh from Mount St. Helens. J. Geophys. Res. 88, 3919–3921. https://doi.org/10.1029/JC088iC06p03919

Iguchi, M., Tameguri, T., Ohta, Y., Ueki, S., Nakao, S., 2013. Characteristics of volcanic vctivity at Sakurajima Volcano's Showa Crater during the period 2006 to 2011(Sakurajima Special Issue). Bull. Volcanol. Soc. Japan. https://doi.org/10.18940/kazan.58.1_115

Iguchi, M., Yakiwara, H., Tameguri, T., Hendrasto, M., Hirabayashi, J. ichi, 2008. Mechanism of explosive eruption revealed by geophysical observations at the Sakurajima, Suwanosejima and Semeru volcanoes. J. Volcanol. Geotherm. Res. 178, 1–9. https://doi.org/10.1016/j.jvolgeores.2007.10.010

Iversen, J.D., Rasmussen, K.R., 1994. The effect of surface slope on saltation threshold. Sedimentology 41, 721–728. https://doi.org/10.1111/j.1365-3091.1994.tb01419.x

Iversen, J.D., Rasmussen, K.R., 1999. The effect of wind speed and bed slope on sand transport. Sedimentology 46, 723–731. https://doi.org/10.1046/j.1365-3091.1999.00245.xIversen, J.D., White, B.R., 1982. Saltation threshold on Earth, Mars and Venus. Sedimentology 29, 111–119. https://doi.org/10.1111/j.1365-3091.1982.tb01713.x

Johnson, K.L., Kendall, K., Roberts, A.D., 1971. Surface energy and the contact of elastic solids. Proc. R. Soc. London. A. Math. Phys. Sci. https://doi.org/10.1098/rspa.1971.0141

Leadbetter, S.J., Hort, M.C., Von Lwis, S., Weber, K., Witham, C.S., 2012. Modeling the resuspension of ash deposited during the eruption of Eyjafjallajökull in spring 2010. J. Geophys. Res. Atmos. 117, 1–13. https://doi.org/10.1029/2011JD016802

Liu, E.J., Cashman, K. V., Beckett, F., Witham, C.S., Leadbetter, S.J., Hort, M.C., Guðmundsson, S., 2014. Ash mists and brown snow: Remobilization of volcanic ash from recent Icelandic eruptions. J. Geophys. Res. Atmos. 119, 1–18. https://doi.org/10.1002/2014JD021598

Macpherson, T., Nickling, W.G., Gillies, J.A., Etyemezian, V., 2008. Dust emissions from undisturbed and disturbed supply-limited desert surfaces. J. Geophys. Res. Earth Surf. 113. https://doi.org/10.1029/2007JF000800

Marticorena, B., Bergametti, G., 1995. Modeling the atmospheric dust cycle: 1. Design of a soil-derived dust emission scheme. J. Geophys. Res. Atmos. 100, 16415–16430. https://doi.org/10.1029/95JD00690

Mejia, J.F., Gillies, J.A., Etyemezian, V., Glick, R., 2019. A very-high resolution (20m) measurement-based dust emissions and dispersion modeling approach for the Oceano Dunes, California. Atmos. Environ. 218, 116977. https://doi.org/10.1016/j.atmosenv.2019.116977

Merrison, J.P., 2012. Sand transport, erosion and granular electrification. Aeolian Res. 4, 1–16. https://doi.org/10.1016/j.aeolia.2011.12.003

Merrison, J.P., Gunnlaugsson, H.P., Nørnberg, P., Jensen, A.E., Rasmussen, K.R., 2007. Determination of the wind induced detachment threshold for granular material on Mars using wind tunnel simulations. Icarus 191, 568–580. https://doi.org/10.1016/j.icarus.2007.04.035

Miwa, T., Geshi, N., Shinohara, H., 2013. Temporal variation in volcanic ash texture during a vulcanian eruption at the sakurajima volcano, Japan. J. Volcanol. Geotherm. Res. 260, 80–89. https://doi.org/10.1016/j.jvolgeores.2013.05.010

Miwa, T., Nagai, M., Kawaguchi, R., 2018. Resuspension of ash after the 2014 phreatic eruption at Ontake volcano, Japan. J. Volcanol. Geotherm. Res. 351, 105–114. https://doi.org/10.1016/j.jvolgeores.2018.01.003

Nickling, W.G., Gillies, J.A., 1989. Emission of fine-grained particulates from desert soils, in: Paleoclimatology and Paleometeorology: Modern and Past Patterns of Global Atmospheric Transport. https://doi.org/10.1007/978-94-009-0995-3_5

Panebianco, J.E., Mendez, M.J., Buschiazzo, D.E., Bran, D., Gaitán, J.J., 2017. Dynamics of volcanic ash remobilisation by wind through the Patagonian steppe after the eruption of Cordón Caulle, 2011. Sci. Rep. 7, 45529. https://doi.org/10.1038/srep45529

Pietersma, D., Stetler, L.D., Saxton, K.E., 1996. Design and aerodynamics of a portable wind tunnel for soil erosion and fugitive dust research. Trans. Am. Soc. Agric. Eng. 39, 2075–2083. https://doi.org/10.13031/2013.27710

Pistolesi, M., Cioni, R., Bonadonna, C., Elissondo, M., Baumann, V., Bertagnini, A., Chiari, L.,

Gonzales, R., Rosi, M., Francalanci, L., 2014. Complex dynamics of small-moderate volcanic events: the example of the 2011 rhyolitic Cordón Caulle eruption, Chile. Bull. Volcanol. 77. https://doi.org/10.1007/s00445-014-0898-3

Poulidis, A.P., Takemi, T., Shimizu, A., Iguchi, M., Jenkins, S.F., 2018. Statistical analysis of dispersal and deposition patterns of volcanic emissions from Mt. Sakurajima, Japan. Atmos. Environ. 179, 305–320. https://doi.org/10.1016/j.atmosenv.2018.02.021

Reckziegel, F., Bustos, E., Mingari, L., Báez, W., Villarosa, G., Folch, A., Collini, E., Viramonte, J., Romero, J., Osores, S., 2016. Forecasting volcanic ash dispersal and coeval resuspension during the April-May 2015 Calbuco eruption. J. Volcanol. Geotherm. Res. 321, 44–57. https://doi.org/10.1016/j.jvolgeores.2016.04.033

Schneider, C.A., Rasband, W.S., Eliceiri, K.W., 2012. NIH Image to ImageJ: 25 years of image analysis. Nat. Methods. https://doi.org/10.1038/nmeth.2089

Shao, Y., Lu, H., 2000. A simple expression for wind erosion threshold friction velocity. J. Geophys. Res. 105, 22437. https://doi.org/10.1029/2000JD900304

Sirjani, E., Sameni, A., Moosavi, A.A., Mahmoodabadi, M., Laurent, B., 2019. Portable wind tunnel experiments to study soil erosion by wind and its link to soil properties in the Fars province, Iran. Geoderma 333, 69–80. https://doi.org/10.1016/j.geoderma.2018.07.012

Suh, S.H., Maki, M., Iguchi, M., Lee, D.I., Yamaji, A., Momotani, T., 2019. Free-fall experiments of volcanic ash particles using a 2-D video disdrometer. Atmos. Meas. Tech. 12, 5363–5379. https://doi.org/10.5194/amt-12-5363-2019

Sweeney, M., Etyemezian, V., Macpherson, T., Nickling, W., Gillies, J., Nikolich, G., McDonald, E.,

2008. Comparison of PI-SWERL with dust emission measurements from a straight-line field wind tunnel. J. Geophys. Res. Earth Surf. 113, 1–12. https://doi.org/10.1029/2007JF000830

Thorsteinsson, T., Jóhannsson, T., Stohl, A., Kristiansen, N.I., 2012. High levels of particulate matter in Iceland due to direct ash emissions by the Eyjafjallajökull eruption and resuspension of deposited ash. J. Geophys. Res. Solid Earth 117, 1–9. https://doi.org/10.1029/2011JB008756

Van Pelt, R.S., Zobeck, T.M., 2013. Portable Wind Tunnels for Field Testing of Soils and Natural Surfaces. Wind Tunn. Des. Their Divers. Eng. Appl. https://doi.org/10.5772/54141

Van Pelt, R.S., Zobeck, T.M., Baddock, M.C., Cox, J.J., 2010. Design, construction, and calibration of a portable boundary layer wind tunnel for field use. Trans. ASABE 53, 1413–1422.

White, F.M., 1991. Viscous Fluid Flow. McGraw Hill, New York.Wilson, T.M., Cole, J.W., Stewart, C., Cronin, S.J., Johnston, D.M., 2011. Ash storms: Impacts of wind-remobilised volcanic ash on rural communities and agriculture following the 1991 Hudson eruption, southern Patagonia, Chile. Bull. Volcanol. 73, 223–239. https://doi.org/10.1007/s00445-010-0396-1

Figure 1

Click here to download high resolution image

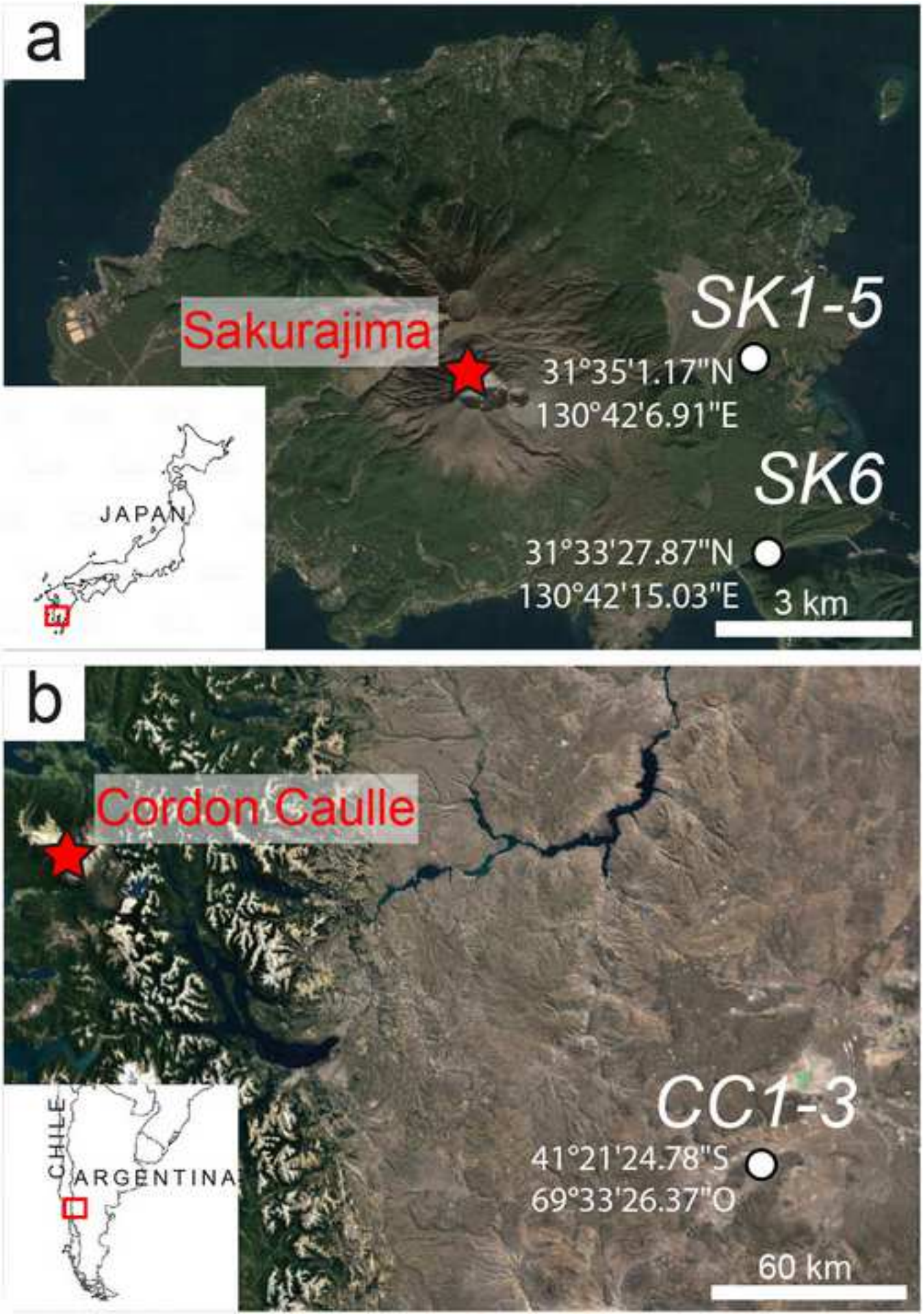

Figure 2

Click here to download high resolution image

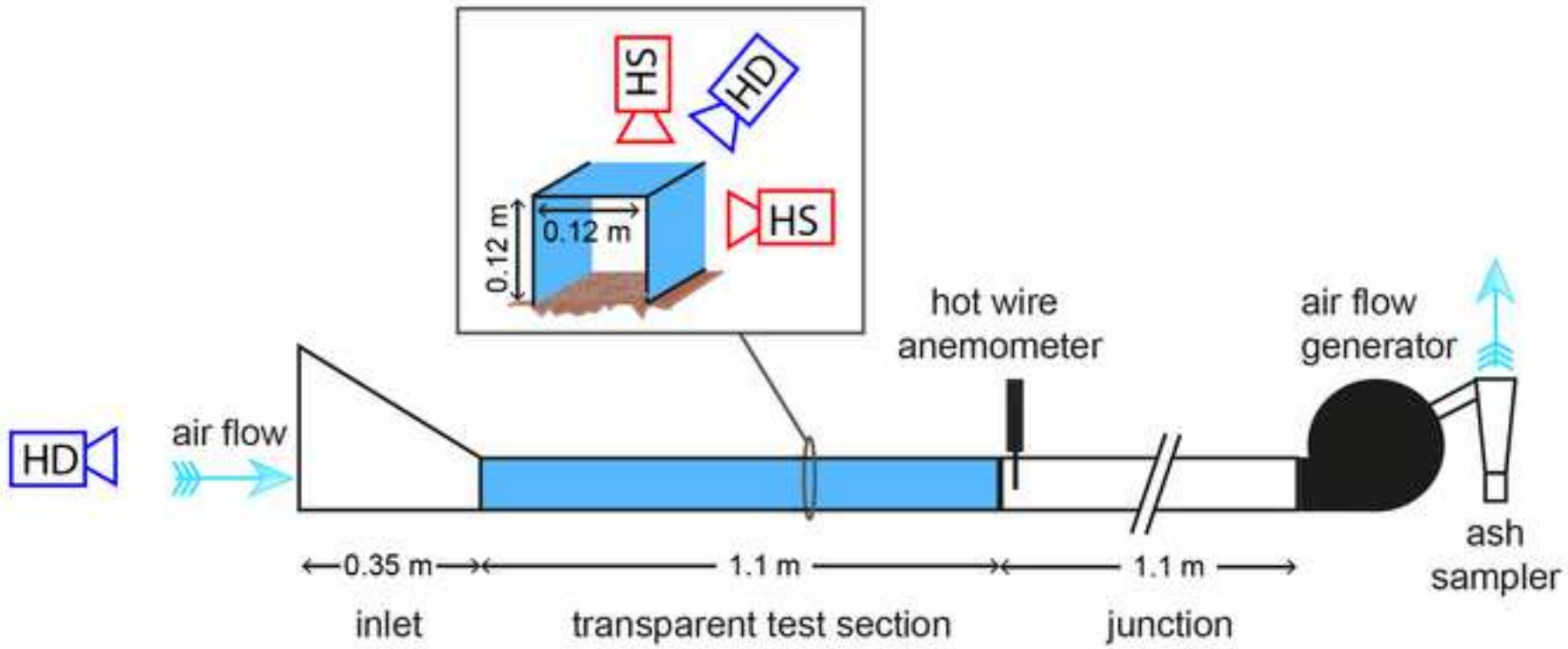

Figure 3

Click here to download high resolution image

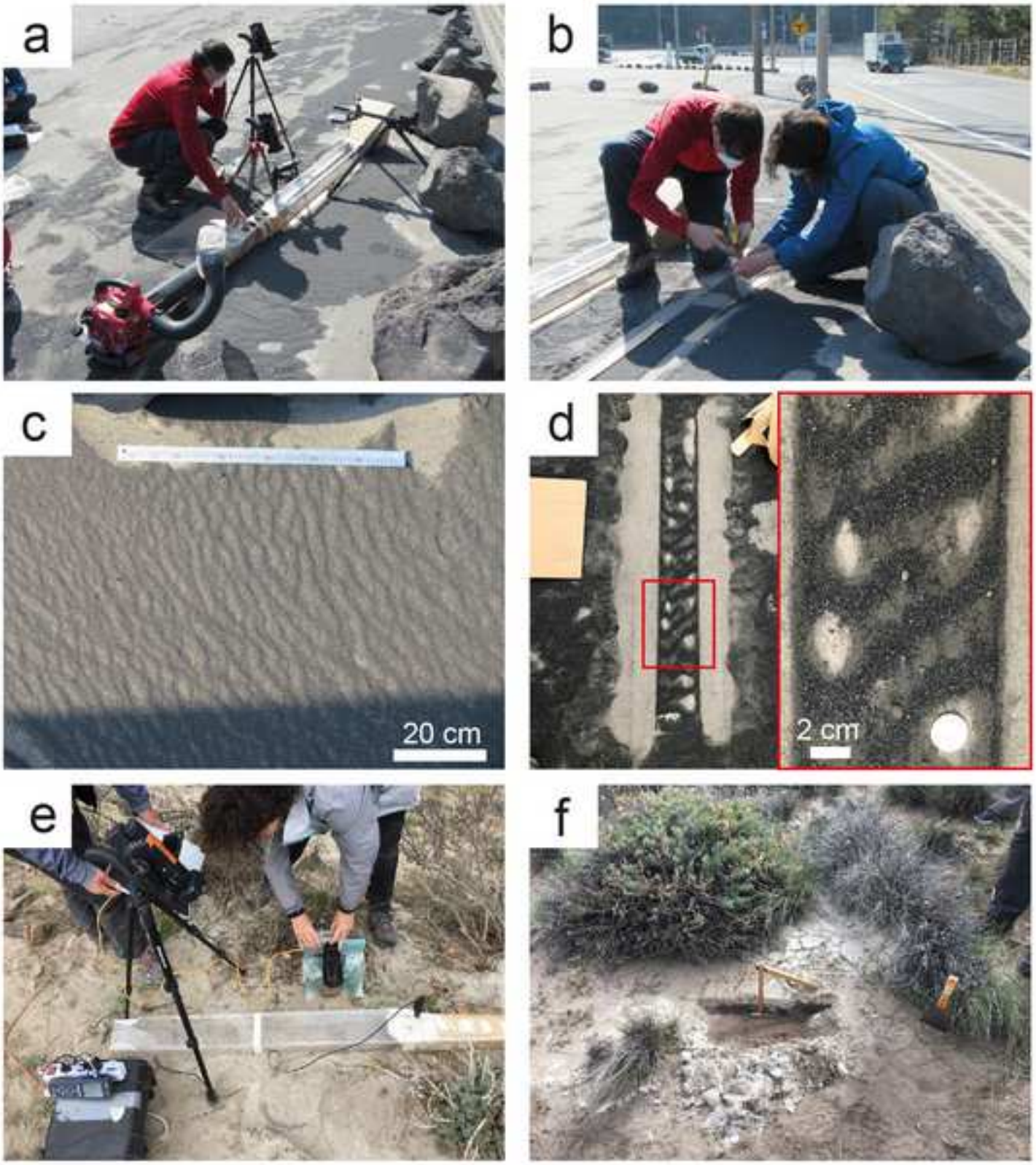

Figure 4

Click here to download high resolution image

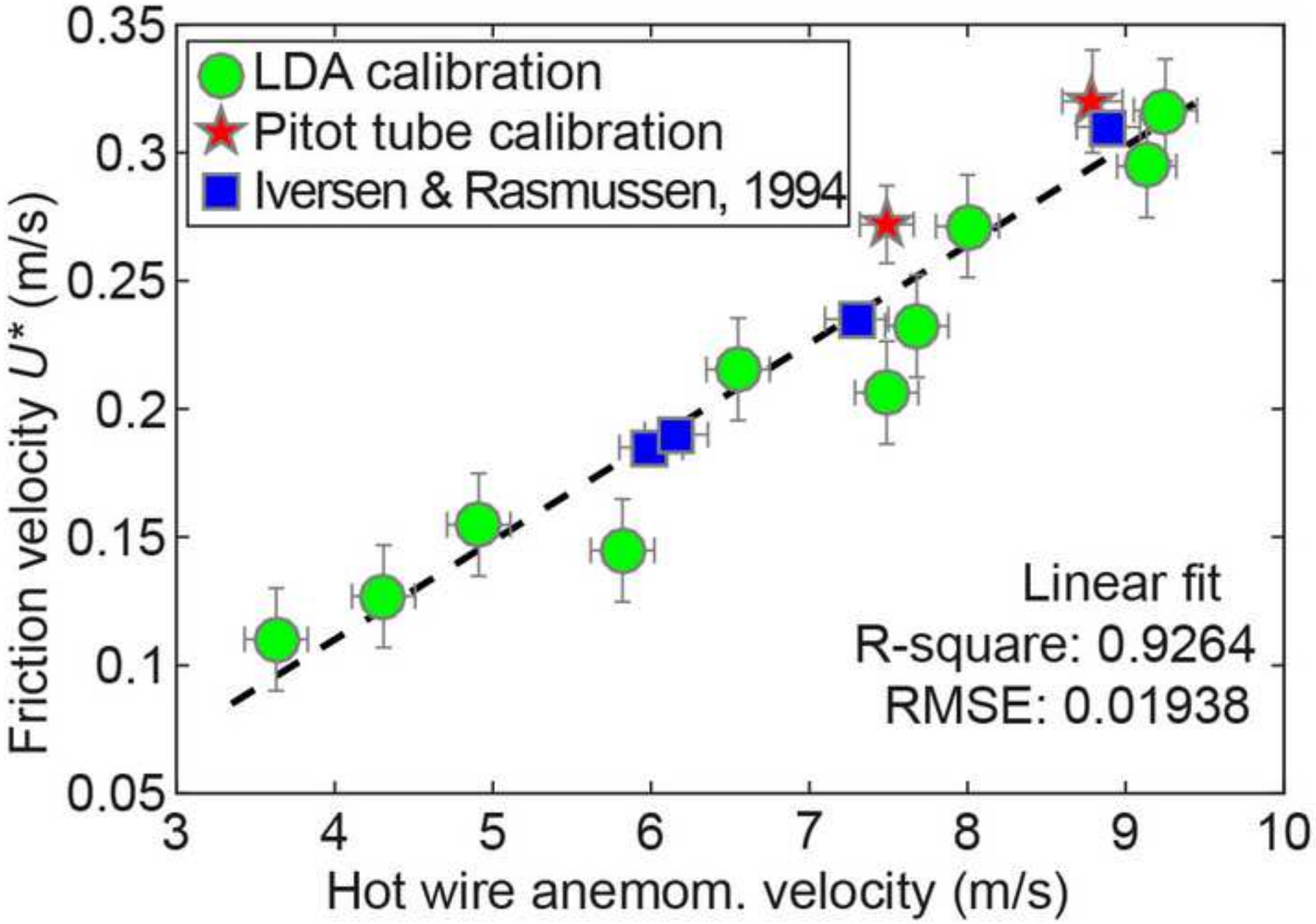

Figure 5

Click here to download high resolution image

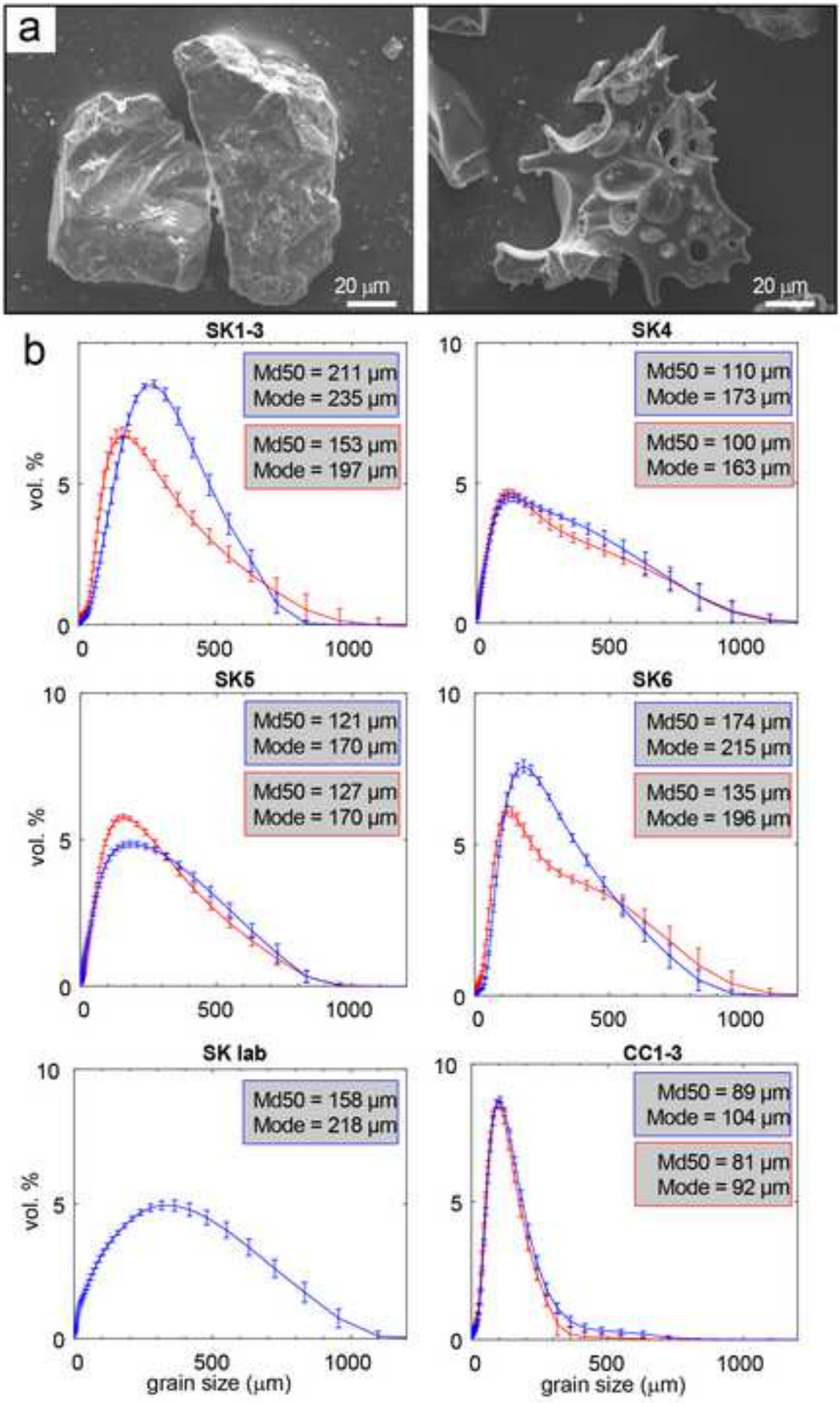

Figure 6

Click here to download high resolution image

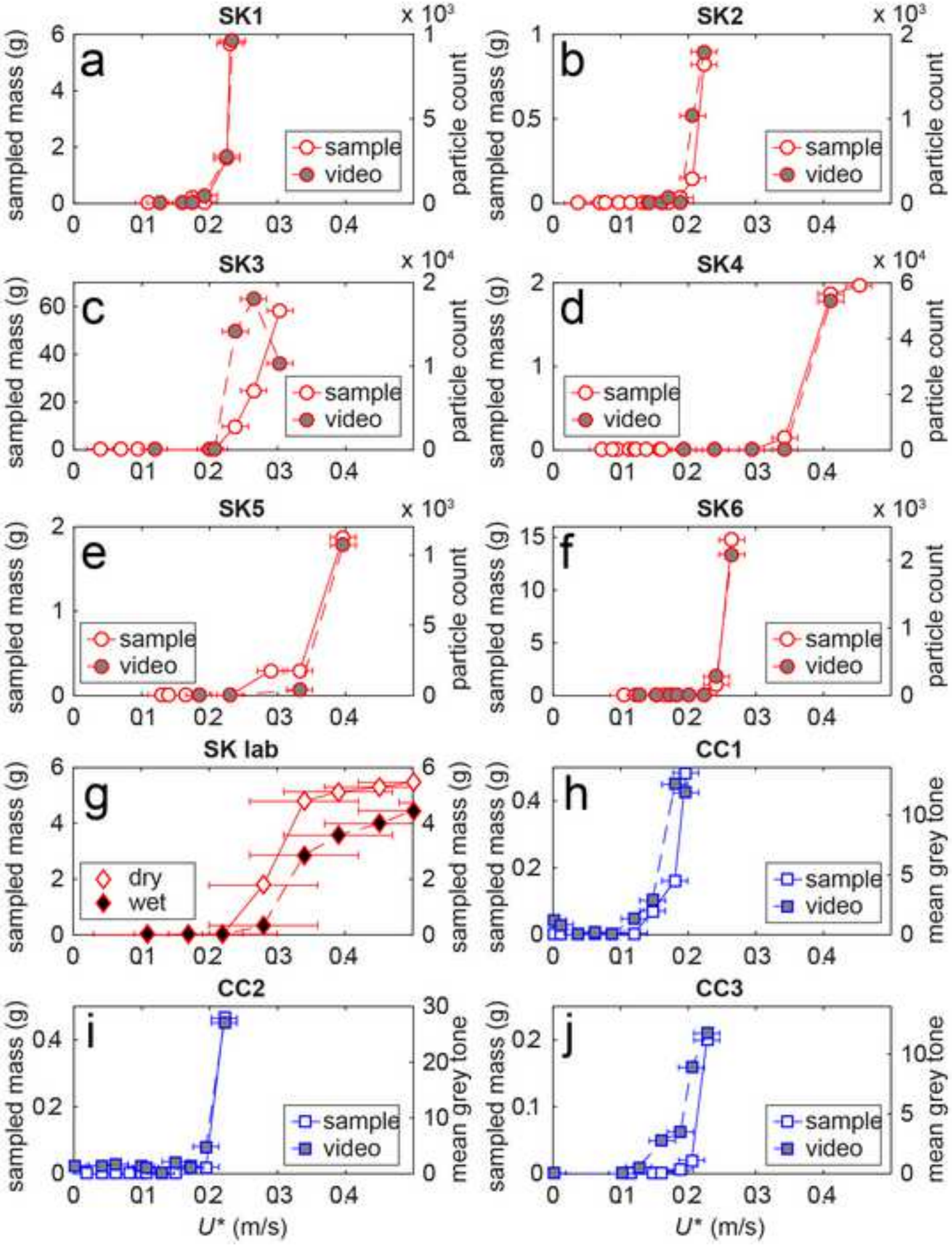

Figure 7

Click here to download high resolution image

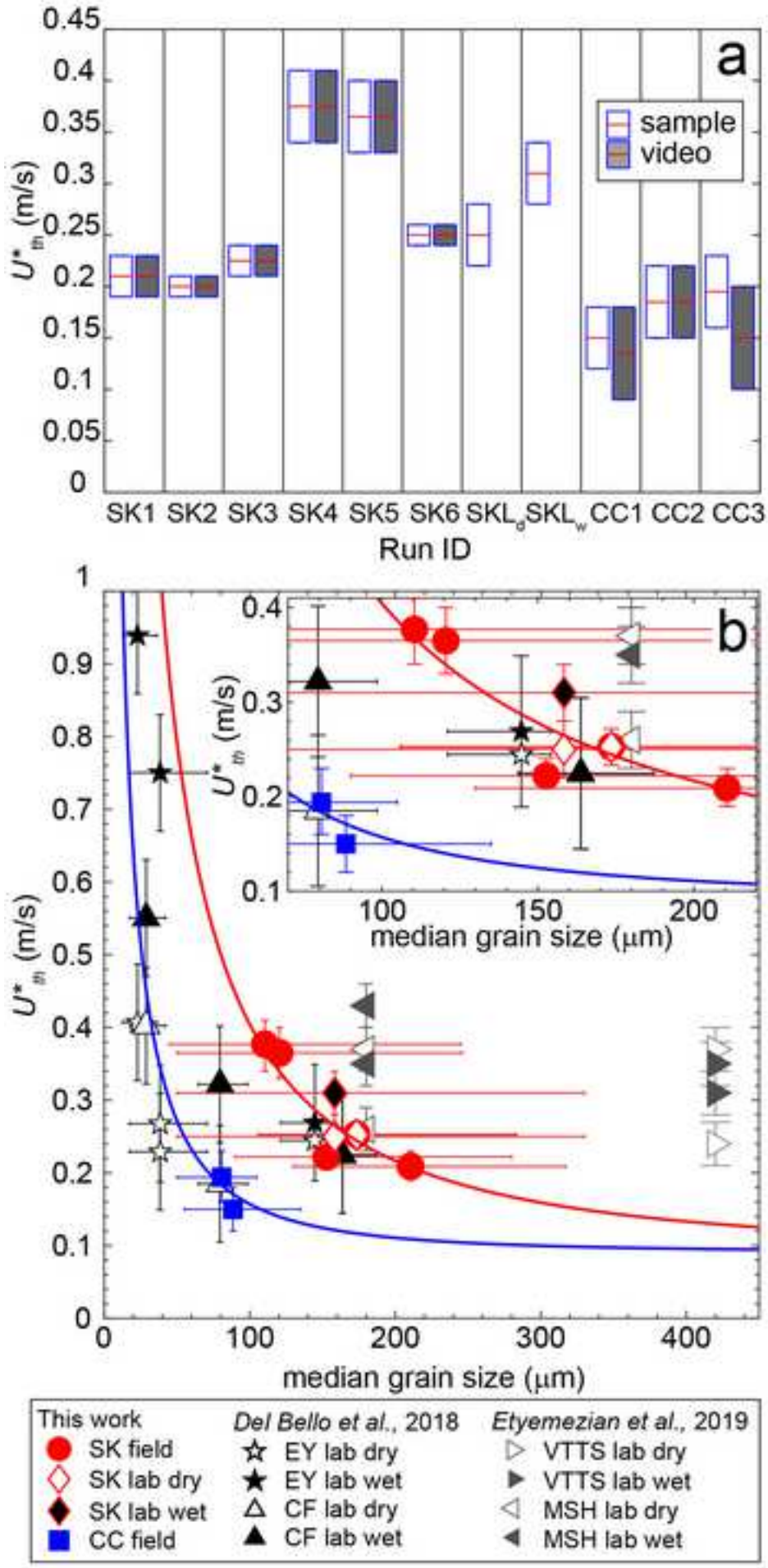

Video 1

Click here to download Supplementary material (video): Video_1.wmv

Video 2

Click here to download Supplementary material (video): Video_2.wmv

***Declaration of Interest Statement**

Declaration of interests

☒ The authors declare that they have no known competing financial interests or personal relationships that could have appeared to influence the work reported in this paper.

☐The authors declare the following financial interests/personal relationships which may be considered as potential competing interests:

CRediT author statement

EDB: Conceptualization, Methodology, investigation, Data Curation, Writing-Original draft. **JT**: Conceptualization, Methodology, investigation, Data Curation, Writing-Original draft. **JPM**: Methodology, Resources, Investigation, Review and Editing. **KRR***:* Methodology, Resources, Investigation, Review and Editing. **DA**: Investigation, resources, funding acquisition. **TR:** investigation, resources. **PS:** Investigation, Resources, Supervision, funding acquisition. **JJI**: Resources, Methodology